Optics Communications 314 (2014) 57–65

Contents lists available at ScienceDirect

Optics Communications

journal homepage: www.elsevier.com/locate/optcom

Near-field radiative heat transfer for Si based metamaterials

Baoan Liu, Jiawei Shi, Kaiyang Liew, Sheng Shen *

Department of Mechanical Engineering, Carnegie Mellon University, Pittsburgh, PA 15213, USA

ARTICLE INFO

Article history:
Received 14 April 2013
Received in revised form
24 May 2013
Accepted 13 October 2013
Available online 31 October 2013

Keywords:
Near-field thermal radiation
Si nanowire array
Si nanohole array

ABSTRACT

Radiative heat transfer in the near field can exceed the blackbody radiation limit by orders of magnitude due to energy transfer through evanescent waves. Doped Si has attracted significant attention in studies of near field thermal radiation, since it is a Drude-type material whose plasma frequency can be tuned into the infrared range by modifying the dopant concentration. Thus, doped Si can serve as a "tunable metal" which can be used to design tunable metamaterials to control near field thermal radiation. In this paper, we study near field radiative heat transfer for two doped Si based metamaterials: Si nanowire arrays and Si nanohole arrays, using fluctuational electrodynamics and effective medium theory.

1. Introduction

Radiative heat transfer plays an important role in a variety of applications such as infrared imaging, energy conversion, thermal insulation, thermal signature control, and thermal management. In terms of the spacing between objects, radiative heat transfer can be categorized into two regimes. In the far-field regime, where the gap size between objects is much larger than the thermal wavelength λth predicted by Wien's displacement law, radiative heat transfer essentially tailors blackbody radiation, which is the maximum radiative transfer given by the Stefan–Boltzmann law for total heat flux and Planck's law for spectral flux. In contrast, radiative heat transfer in the near-field regime, in which the gap size is smaller than λth, can be dramatically enhanced beyond blackbody radiation due to the tunneling of evanescent waves. In particular, near-field radiative heat transfer can be increased by several orders of magnitude as compared to blackbody radiation, when interacting materials support resonant surface waves in the infrared range, for example, surface phonon polaritons in polar dielectrics (e.g., BN, SiC or SiO_2). Although the spectral resonances of surface phonon polaritons usually exist at fixed frequencies for polar dielectrics, the plasma frequency of doped semiconductors can be continuously tuned in the infrared range by adjusting their dopant concentrations, thus provide exciting opportunities for controlling near-field radiative heat transfer.

Clearly, in order to achieve the control of near-field radiative heat transfer, tuning infrared radiative properties of materials is the key. Over the past decade, electromagnetic metamaterials, in which the structure features are much smaller than the working wavelength of light, have offered an entirely new paradigm for designing special electromagnetic properties (e.g., negative refraction, electrical and magnetic resonances) and manipulating the interactions between light and materials [1–3]. In metamaterials, the representative unit cell size is much smaller than wavelength so that the optical properties of metamaterials can be modeled by effective medium theory. In this work, we will focus on two types of widely used Si nanostructures or metamaterials: Si nanohole arrays (SiHAs) and Si nanowire arrays (SiWAs). The near-field radiative properties of these Si based metamaterials and thus radiative heat transfer can be tuned by changing the dopant concentration of Si and the filling ratio of nanoholes or nanowires.

2. Mathematical formulation of near-field radiative heat transfer

Thermal radiation is caused by thermally induced fluctuating currents inside materials. The correlation between the material temperature and the average intensity of the fluctuating currents can be described by fluctuational electrodynamics [4,5]

$$\langle J_{\mathbf{k}}(r,\omega)J^{*}_{\mathbf{l}}(r',\omega')\rangle = F(\omega,T)\delta(\omega-\omega')\delta_{\mathbf{kl}}\delta(r-r'), \quad (1)$$

where $F(\omega,T)=4\varepsilon_0\mathrm{Im}[\varepsilon_r]\Theta(\omega,T)/\pi$ is a deterministic function, the bracket $\langle\cdot\rangle$ denotes the statistical ensemble average, ε_0 is the permittivity of vacuum, $\mathrm{Im}[\varepsilon_r]$ is the imaginary part of the dielectric function of the object, and $\Theta(\omega,T)=\hbar\omega/[exp(\hbar\omega/k_BT)-1]$ is the Planck distribution which represents the mean energy of a harmonic oscillator. $\delta_{\mathbf{kl}}\delta(r-r')$ are the Kronecker delta and Dirac delta functions that indicate the random currents are incoherent at different polarizations ($\mathbf{l}$ and $\mathbf{k}$) and different locations, respectively. $\delta(\omega-\omega')$ indicates the temporal incoherence. The radiative heat flux from a thermal source can be evaluated by the average Poynting vector,

* Corresponding author. Tel.: +1 412 268 3393.
E-mail address: sshen1@cmu.edu (S. Shen).

0030-4018/$ - see front matter © 2013 Elsevier B.V. All rights reserved.
http://dx.doi.org/10.1016/j.optcom.2013.10.074

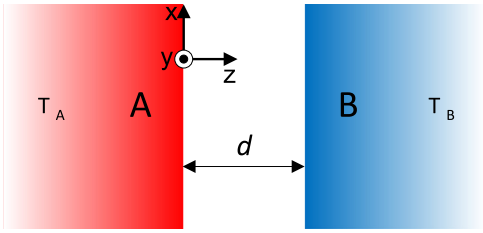

Fig. 1. Two semi-infinite bodies A and B separated by a vacuum gap d, which are maintained at different temperatures T_A and T_B, respectively.

which is a deterministic value according to Eq. (1)

$$\Phi(r,\omega)=\left\langle\frac{1}{2}\mathrm{Re}[E(r,\omega)\times H^*(r,\omega)]\right\rangle$$
$$=i\mu_0\omega\int_V dr'\int_V dr''G^{EE}(r,r')G^{HE*}(r,r'')\langle J(r')J^*(r'')\rangle$$
$$=i\mu_0\omega F\int_V dr'G^{EE}(r,r')G^{HE*}(r,r'), \quad (2)$$

where G^{EE}, G^{HE} are the dyadic Green's functions that denote the electric and magnetic responses to a single dipole source, respectively [6].

As shown in Fig. 1, two semi-infinite bodies A and B with temperatures T_A, T_B, respectively, are separated by a vacuum gap d. From fluctuational electrodynamics, the radiative heat flux $\Phi_{A\to B}$ from A to B can be evaluated analytically as [7]

$$\Phi_{A\to B}=\int_0^\infty\frac{d\omega}{2\pi}[\Theta(\omega,T_A)-\Theta(\omega,T_B)]\sum_{j=s,p}\int\frac{d^2\mathbf{K}}{4\pi^2}T_j^{AB}(\omega,K,d), \quad (3)$$

where $\mathbf{K}=(k_x,k_y)$ is the transverse component of wavevector, $K=|\mathbf{K}|$ is the norm of $\mathbf{K}$, the integral for $\mathbf{K}$ is carried out over both the propagating wave regime ($K\le k_0$) and the evanescent wave regime $K>k_0$. $j=\{s,p\}$ denotes the s- and p- polarized wave components. $T_j^{AB}\in[0,1]$ is the transmission factor (TF) presented in Ref. [7]. In our case, it can be expressed as

$$T_j^{AB}(\omega,K,d)=\begin{cases}\frac{(1-|r_j^A|^2)(1-|r_j^B|^2)}{|1-r_j^Ar_j^B\exp(2ik_{0z}d)|^2} & K\le k_0\\ \frac{4\mathrm{Im}(r_j^A)\mathrm{Im}(r_j^B)\exp(-2\mathrm{Im}[k_{0z}]d)}{|1-r_j^Ar_j^B\exp(2ik_{0z}d)|^2} & K>k_0\end{cases}, \quad (4)$$

where k_0 is free-space wavevector, r_j is the Fresnel reflection coefficient of body A or B, $k_{0z}=\sqrt{k_0^2-K^2}$ is the component of wavevector in vacuum along the surface normal of the plate.

When a radiative photon transmits across the vacuum gap, its polarization, frequency and transverse wavevector always remain the same. Thus, the photons can be classified into different transmission modes $(j,\omega,\mathbf{K})$. Physically, the transmission factor can be understood as the probability of photons transmitting from A to B through mode $(j,\omega,\mathbf{K})$. $K\le k_0$ corresponds to the transmission modes of propagating waves, and $K>k_0$ corresponds to the transmission modes of evanescent waves. Therefore, we can see that Eq. (3) predicts the radiative heat transfer in both far-field and near-field thermal radiation regimes.

Radiative heat transfer can be greatly enhanced in the near-field regime due to the enormous contribution from the transmission modes of evanescent waves. For the far-field thermal radiation, the gap d between A and B is too large in comparison with the thermal wavelength, which makes the exponential term of evanescent waves in the TF negligible. However, for near-field thermal radiation, in which d is smaller than the thermal wavelength, the contribution from the transmission modes of evanescent waves cannot be ignored. In some cases, it could dominate the heat transfer which can exceed the blackbody radiation limit predicted by the Stefan–Boltzmann law by several orders of magnitude [5,7,8]. In fact, the Stefan–Boltzmann law can be derived from Eq. (3) by setting $T_j^{AB}=1$ for all propagating waves and $T_j^{AB}=0$ for all evanescent waves. Thus, it is not surprising that the blackbody limit breaks down in the near-field. According to the explanation based on TF, a blackbody rejects all the incident photons in the transmission modes of evanescent waves.

TF formalism clarifies the transmissivity of evanescent waves in radiative heat transfer. Previous work [7,9] has successfully applied the TF formalism to quantitatively explain the mechanism of near-field radiative heat transfer for both resonant and non-resonant materials. The qualitative picture of the TF formalism can be illustrated by the "weighted TF" formalism mentioned in Ref. [10], for the geometries which are symmetric in the transverse (i.e., x–y) directions. Since the photon transmission modes $(j,\omega,\mathbf{K})$ with the same norm $K=|\mathbf{K}|$ cannot be distinguished due to the incoherence of the thermal radiation, we express the weighted TF as Y_j^{AB} in the "weighted phase space" (j,ω,K_r) with $K_r=K/k_0$, which has the form

$$\Phi_{A\to B}=\int_0^\infty\frac{d\omega}{2\pi}[\Theta(\omega,T_A)-\Theta(\omega,T_B)]\sum_{j=s,p}\int_0^\infty dK_r\left[\frac{k_0^2K_r}{2\pi}T_j^{AB}(\omega,k_0K_r,d)\right]$$
$$=\int_0^\infty\frac{d\omega}{2\pi}[\Theta(\omega,T_A)-\Theta(\omega,T_B)]\sum_{j=s,p}\int_0^\infty dK_rY_j^{AB}(\omega,K_r,d). \quad (5)$$

Thus, Y_j^{AB} qualitatively represents the contribution of the photon transmission modes $(j,\omega,\mathbf{K}|K=K_rk_0)$ to the total radiative heat transfer between bodies A and B. Furthermore, in the weighted phase space, the propagating and evanescent wave modes are separated by a straight line $K_r=1$.

Likewise, the photon local density of states (LDOS) above a body can also be expressed in the weighted phase space. In near-field thermal radiation, LDOS is proposed to estimate the evanescent wave emissivity/absorptivity of a body [11]. Conventionally, the LDOS is defined to determine the radiation rate of a dipole near a body [6]. For a dipole located very close to a body, its radiation rate can be greatly enhanced in comparison with a dipole located in the homogenous vacuum space, since the radiation in this case is dominated by the energy transfer through evanescent photons. Therefore, the LDOS can be used to qualitatively estimate the evanescent wave absorptivity (which is equivalent to emissivity) of the body in near-field thermal radiation.

According to Ref. [6], the LDOS can be calculated as

$$\rho(r,\omega)=\frac{U(r,\omega)}{\Theta(\omega,T)}, \quad (6)$$

where $U(r,\omega)$ is the thermally induced electromagnetic energy density at point r. Thus, the heat transfer between the two bodies can be qualitatively estimated as

$$\Phi_{A\to B}\sim\int\frac{d\omega}{2\pi}[\Theta(\omega,T_A)-\Theta(\omega,T_B)]\rho_A(d,\omega)\rho_B(d,\omega). \quad (7)$$

For a semi-infinite body, the LDOS at the distance d above its surface can be calculated analytically as [6]

$$\rho(d,\omega)=\frac{\omega^2}{2\pi^2c^3}\left\{\int_0^{k_0}\frac{KdK}{k_0|k_{0z}|}\frac{(1-|r_s|^2)+(1-|r_p|^2)}{2}\right.$$
$$\left.+\int_{k_0}^\infty\frac{4K^3dK}{k_0^3|k_{0z}|}\frac{\mathrm{Im}[r_s]+\mathrm{Im}[r_p]}{2}e^{-2Im[k_{0z}]d}\right\}, \quad (8)$$

which can be rewritten in the weighted phase space as

$$\rho_A(d,\omega)=\int_0^\infty dK_rP(\omega,K_r,d), \quad (9)$$

where we define $P(\omega,K_r,d)$ as the weighted LDOS, which represents the contribution from the photons in the modes $(j,\omega,\mathbf{K}|K=K_rk_0)$ to

the LDOS $\rho(d,\omega)$. Specifically, it can be expressed as

$$P(\omega,K_r,d)=\begin{cases}\frac{\omega^2}{2\pi^2c^3}\frac{K_r k_0}{|k_{0z}|}\frac{(1-|r_s^A|^2)+(1-|r_p^A|^2)}{2} & K_r\le 1\\ \frac{\omega^2}{2\pi^2c^3}\frac{4K_r^3 k_0}{|k_{0z}|}\frac{\mathrm{Im}[r_s^A]+\mathrm{Im}[r_p^A]}{2}e^{-2Im[k_{0z}]d} & K_r>1\end{cases}. \quad (10)$$

According to Eq. (7), the weighted transmission factor $Y^{AB}(\omega,K_r)$ can thus be estimated as

$$Y^{AB}(\omega,K_r)\sim P^A(\omega,K_r,d)P^B(\omega,K_r,d) \quad (11)$$

In this paper, we apply the aforementioned weighted LDOS formalism to study the near-field thermal radiation properties of Si based anisotropic metamaterials such as SiWAs and SiHAs.

3. Optical properties of doped Si

The optical properties of doped Si are reviewed as follows. The Drude model is used to describe the dielectric function of doped Si [12]

$$\epsilon_{Si}(\omega)=\epsilon_{bl}-\frac{N_e e^2/\epsilon_0 m_e^*}{\omega^2+i\omega/\tau_e}-\frac{N_h e^2/\epsilon_0 m_h^*}{\omega^2+i\omega/\tau_h}, \quad (12)$$

where the first term on the right hand side ϵ_{bl} represents the dielectric function of intrinsic Si, which can be taken as a constant equal to 11.7 in the infrared range ($\lambda>2$ μm) [5]. The second term is the Drude term for transitions in the conduction band (free electrons). The third term is the Drude term for transitions in the valence band (free holes). N_e and N_h are the carrier concentrations for electrons and holes, m_e^* and m_h^* are the effective masses of electrons and holes for conductivity calculation, and τ_e and τ_h are scattering times for free electrons and holes. In our simulation, we take the values of effective mass as $m_e^*=0.27m_0$ and $m_h^*=0.37m_0$, where m_0 is free electron mass [12].

It can be seen from Eq. (12) that it is necessary to determine carrier concentrations (N_e and N_h) and scattering times (τ_e and τ_h) in order to obtain a proper expression for $\epsilon(\omega)$. When the dopant concentration is low, complete ionization can be achieved. However, when the dopant concentration is very high ($>10^{19}/\mathrm{cm}^3$), the dopants cannot be completely ionized. In this calculation, a general analysis is used to account for both complete and incomplete ionizations based on charge neutrality [13]. This method is valid for both non-degenerately and degenerately doped Si. The correlation between the dopant concentration and the carrier concentration takes the value mentioned in Ref. [12]. The scattering time used in this work is obtained from the empirical expression for mobility [14]

$$\mu=\mu_{\min}+\frac{\mu_{\max}-\mu_{\min}}{1+(N_d/N_r)^{\alpha}}, \quad (13)$$

where μ is the mobility of electrons or holes, μ_{min}, μ_{max}, α and N_r are the fitting parameters, N_d is the dopant concentration. For different dopants, these parameters are different. The Si used in our simulation is assumed to be arsenic n-doped, for which $\mu_{min}=52.2$ cm^2/V-s, $\mu_{max}=1417$ cm^2/V-s, $\alpha=9.68\times10^{16}$ and $N_r=0.68$. The temperature is maintained at 300 K. In this paper, we consider the cases with the dopant concentration $N_d<10^{21}\mathrm{cm}^{-3}$, corresponding to carrier concentration $N_e<4\times10^{19}\mathrm{cm}^{-3}$, according to Ref. [12].

We plot the permittivity of Si with different dopant concentrations in Fig. 2. By evaluating the sign of the real part of the permittivity, we can see that doped Si behaves like a metal at low frequency and like a dielectric at high frequency. In addition, the material property of doped Si can be tuned by changing the dopant concentrations, since the plasma frequency of the doped Si relates to the doping level, according to Eq. (12).

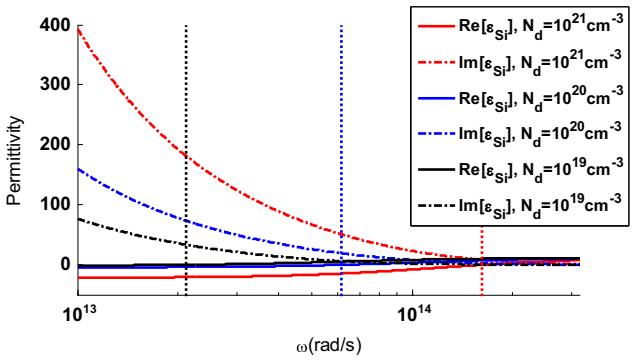

Fig. 2. The permittivity of doped Si at different dopant concentrations. Solid and dashed curves represent the real and imaginary parts of the permittivity, respectively. The vertical dotted line denotes the boundary between the metallic and dielectric material properties (left side is metallic property ($\mathrm{Re}[\epsilon]<0$), and right side is dielectric property ($\mathrm{Re}[\epsilon]>0$)).

4. Near-field thermal radiation of bulk doped Si

We investigate the "near-field absorptivity/emissivity" of semi-infinite doped Si plates with different dopant concentrations by evaluating their weighted LDOS at distance $d=10$ nm above them. Based on the concept mentioned in Ref. [7], the white solid and dashed lines in Fig. 3 divide the photon modes (ω,K_r) into three different regions: (1) propagating photon modes with $K_r<1$, which correspond to the propagating photons in both vacuum and doped Si; (2) frustrated photon modes with $1<K_r<n_{\mathrm{Si}}$ due to total internal reflection, which correspond to the photons that are evanescent in vacuum but propagating inside doped Si; and (3) evanescent photon modes $K_r>n_{\mathrm{Si}}$, which correspond to the evanescent photons in both vacuum and doped Si. Here, $n_{\mathrm{Si}}=\mathrm{Re}[\sqrt{\epsilon_{\mathrm{Si}}}]$ is the refractive index of doped Si. For radiative heat transfer between two bodies in the near-field, all these three photon modes can contribute to heat transfer. Evanescent photon modes with large K have especially dominant contribution, since large K leads to high density of photon modes $(j,\omega,\mathbf{K})$. We can see from Fig. 3 that the near-field thermal radiation of bulk doped Si is dominated by the evanescent photon modes ($K_r>n_{\mathrm{Si}}$). In addition, the K_r of the dominant photon modes lies around the line of $(k_0d)^{-1}$. This is due to the fact that $\mathrm{Im}[r_p]$ does not have big jumps in the evanescent wave regime for the doped Si cases. Therefore, according to Eq. (10), $P(\omega,K_r,d)$ goes to the maximum at $K_r\approx(k_0d)^{-1}$, since its trend is dominated by the term $(K_r^2/|k_{0z}|)\times\exp[-2\mathrm{Im}[k_{0z}]d]$.

We further scrutinize the physics of the dominant evanescent photon modes in near-field thermal radiation for bulk Si. Previous experiments demonstrated that near-field radiative heat transfer between two polar dielectric bodies (e.g., SiO_2, Al_2O_3) could be greatly enhanced to exceed the blackbody limit by several orders of magnitude [8,15]. Theoretical studies attribute the great enhancement to the energy transfer through coupled surface wave modes on the surfaces of two bodies [5,7]. Surface waves are formed due to the coupling between electromagnetic waves and free charge oscillations (surface plasmon polaritons) in metals, or lattice vibrations (surface phonon polaritons) in polar dielectrics. Since the propagating wavevector K of surface waves can be very large, near-field thermal radiation can be enhanced due to surface waves, for example, surface phonon polaritons in polar dielectrics. Doped Si supports surface plasmon polaritons at low frequency range where $\mathrm{Re}[\epsilon_{\mathrm{Si}}]<-1$. However, unlike the aforementioned polar dielectric materials, near-field thermal radiation of doped Si is not dominated by the surface wave modes. In Fig. 3, most of the dominant photon modes are located in the dielectric property

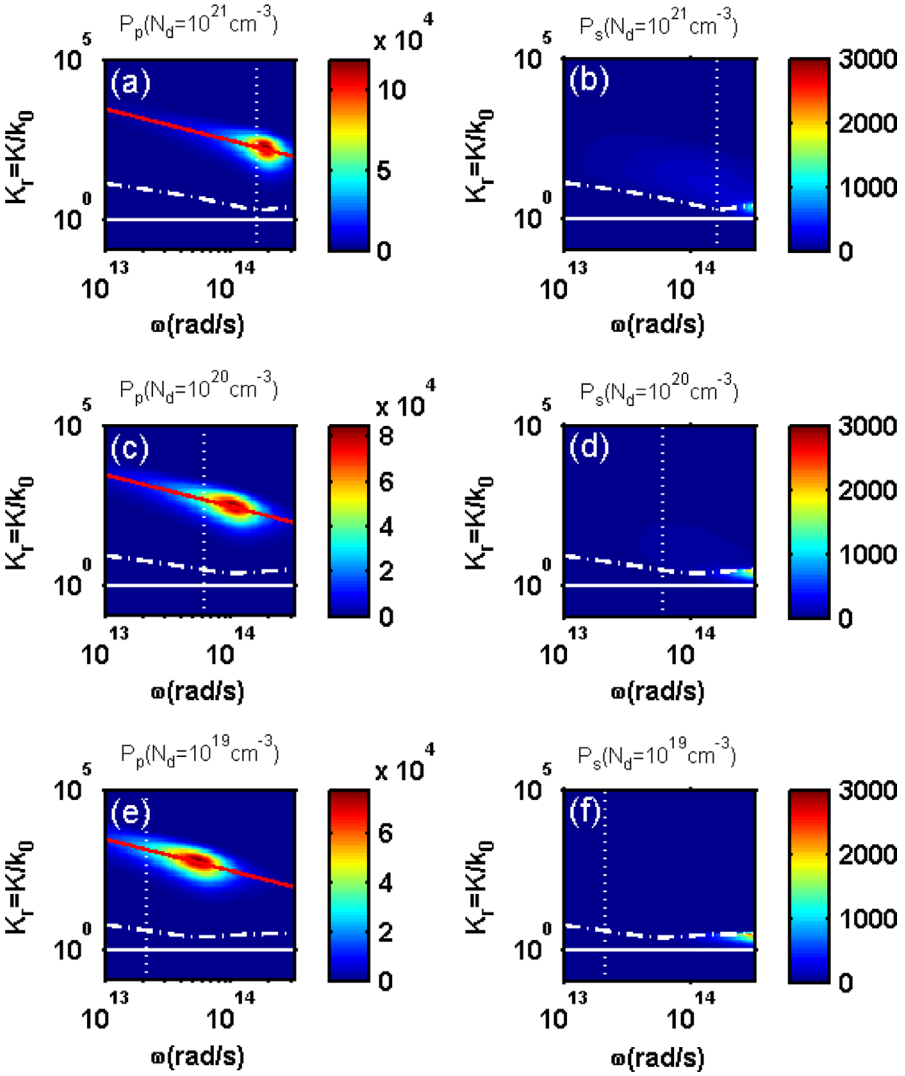

Fig. 3. The weighted LDOS at distance $d=10$ nm from the doped Si semi-infinite plates, with different doping concentrations. Specifically, P_p denotes the contribution from the p-polarized photon modes to the weighted LDOS, and P_s denotes the contribution from the s-polarized photon modes. The white solid lines and dashed lines partition the (ω, K_r) phase space into the regions of $(K<k_0)$, $(k_0<K<n_{Si}k_0)$ and $(K>n_{Si}k_0)$, where $n_{Si}=\mathrm{Re}[\sqrt{\epsilon_{Si}}]$ is the refractive index of the doped Si. The vertical dotted line separates metallic material property (left part) and the dielectric material property (right part) of doped Si. The red curves in (a), (c), (e) plot the function of $(k_0 d)^{-1}$. (For interpretation of the references to color in this figure legend, the reader is referred to the web version of this article.)

region ($\mathrm{Re}[\epsilon]>0$), which prohibits any surface waves modes. Below the plasma frequency of doped Si, the imaginary part of its permittivity is significantly larger than the real part, as shown in Fig. 2. Hence, the surface wave modes in doped Si do not support large K, according to the dispersion relation of the surface waves [6]

$$K = k_0\sqrt{\frac{\epsilon_{Si}}{\epsilon_{Si}+1}}. \tag{14}$$

The near-field thermal radiation of doped Si in our case is mainly attributed to the direct absorption of the evanescent photons incident from vacuum by the induced dipoles beneath the surface of the opposing body. A similar conclusion was also obtained by Ref. [12].

We further study the impact of the imaginary part of ϵ_{Si} on the near field heat transfer between two doped Si plates. Consider the near field heat transfer between two doped Si plates with dopant concentration $N_d=10^{20}\mathrm{cm}^{-3}$ separated by a 10 nm vacuum gap. According to Eq. (12), the relative permittivity of the doped Si can be approximated as

$$\epsilon_{Si} = 11.7 - \frac{\omega_p^2}{\omega^2+i\omega/\tau_e}, \tag{15}$$

where ω_p is the plasma frequency and $\omega_p=4.05\times10^{14}[\mathrm{rad}/s]$, τ_e is the free electron scattering time defined in Section 3, and $\tau_e=\tau_0=9.87\times10^{-15}[\mathrm{s}]$. In order to demonstrate the impact of the imaginary part of ϵ_{Si} (or the loss of the doped Si) on coupled surface wave modes, in Fig. 4, we plotted the weighted TF of the heat transfer between two doped Si plates whose τ_e equals $\tau_0, 2\tau_0, 5\tau_0, 10\tau_0$, respectively. Note that larger τ_e implies the smaller imaginary part of ϵ_{Si}, which also means the lower loss of the doped Si. We also plot the dispersion relation of coupled surface wave modes (fundamental TM modes) for this Si–vacuum–Si structure based on the argument principle method mentioned in Ref. [16].

From Fig. 4, we can see that τ_e controls the contribution from coupled surface wave modes to heat transfer. For the original doped Si case with $\tau_e=\tau_0$ (Fig. 4(a)), the heat transfer is

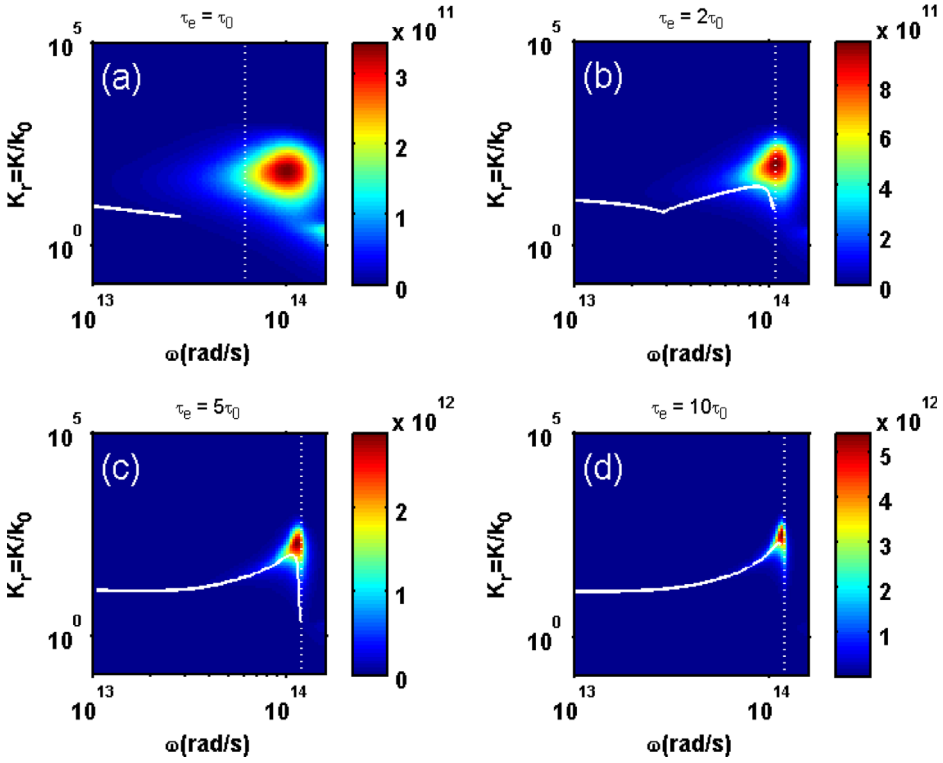

Fig. 4. The weighted TF of the radiative heat transfer between two doped Si plates at different electron scattering times τ_e. The vertical dotted line separates metallic material property (left part) and the dielectric material property (right part) of doped Si. The white solid line denotes the dispersion relation of coupled surface wave modes (fundamental TM modes) of the Si–vacuum–Si structure.

dominated by the photon modes in the dielectric regime, and the contribution from coupled surface wave modes is negligible. However, for the artificial doped Si case with $\tau_e = 10\tau_0$ (Fig. 4 (d)), the dominant photon modes lie in the metallic regime and also overlap the dispersion relation curve of coupled surface wave modes, which means the heat transfer in this case is dominated by the photon transport through coupled surface wave modes. Therefore, we conclude that it is the larger imaginary part (or high loss, or short carrier scattering time) of the doped Si mitigates the contribution from the coupled surface plasmon wave modes to the heat transfer between two Si plates.

The weighted TF of the radiative heat transfer between two bulk doped Si plates at different dopant concentrations is plotted in Fig. 5. In comparison with Fig. 3, we can see that the weighted LDOS qualitatively serves as near-field absorptivity/emissivity of a material. Also, note that the high frequency photons in the frustrated modes have the potential to dominate near-field heat transfer. However, at room temperature $T=300$ K, the contribution from these photon modes can be ignored due to the very low photon population.

5. Near-field thermal radiation of SiWA and SiHA metamaterials

Recently, nanowire arrays based hyperbolic metamaterials have been proposed to enhance near-field thermal radiation. Liu et al. [17] demonstrated a hyperbolic metamaterial based on metallic nanowire arrays which can be used as a broadband near-field thermal emitter. Biehs et al. [9] showed that the radiative heat transfer between two SiC nanowire arrays can exceed the heat transfer between two SiC plates. As illustrated in Fig. 2, the material property of doped Si can be tuned from metal-like properties to dielectric-like properties by changing its dopant concentration. Thus, we are curious to find out if SiWAs can be employed to design tunable hyperbolic metamaterials for controlling near-field thermal radiation. We also study the near-field thermal radiation of SiHAs as a parallel comparison to SiWAs.

The principles of hyperbolic metamaterial mediated near-field thermal radiation are briefly reviewed below. Consider an anisotropic metamaterial (i.e., nanostructures) with effective permittivity in the tensor form

$$\overline{\overline{\epsilon}} = \epsilon_{par}[\mathbf{e_x e_x} + \mathbf{e_y e_y}] + \epsilon_{vet}\mathbf{e_z e_z}, \tag{16}$$

where $\epsilon_{par}, \epsilon_{vet}$ are the parallel and vertical components of its effective permittivity respectively. A hyperbolic metamaterial has its $\mathrm{Re}[\epsilon_{par}]$ and $\mathrm{Re}[\epsilon_{vet}]$ in different signs. There are many designs realizing hyperbolic metamaterials, such as multilayer structures [18,19] and nanowire arrays structures [9,17]. In this paper, we focus on the SiWA hyperbolic metamaterial with $\mathrm{Re}[\epsilon_{par}] > 0$ and $\mathrm{Re}[\epsilon_{vet}] < 0$. Thus, its dispersion relation is a hyperbolic function

$$\frac{k_z^2}{\epsilon_{par}} - \frac{K^2}{-\epsilon_{vet}} = \frac{\omega^2}{c_0^2} = k_0^2, \tag{17}$$

where $K = \sqrt{k_x^2 + k_y^2}$ is the parallel component of the wavevector and k_z is the vertical component of the wavevector. This dispersion relation shows that hyperbolic metamaterials can couple the evanescent photons in vacuum with large K into the propagating wave modes with real k_z. Therefore, the LDOS of hyperbolic metamaterials is expected to be greatly enhanced, since theoretically all the photons with $K > k_0$ can be coupled with propagating waves inside the metamaterial and eventually be absorbed due to material loss. Furthermore, for the nanowire array made from Drude materials (e.g. metal, dope Si, etc.), whose $\mathrm{Re}[\epsilon] < 0$ for the frequency below the plasma frequency, its near-field radiation enhancement could be broadband, since the hyperbolic dispersion can always be satisfied. One example is that metal nanowire arrays can serve as a broadband near-field thermal emitter/absorber,

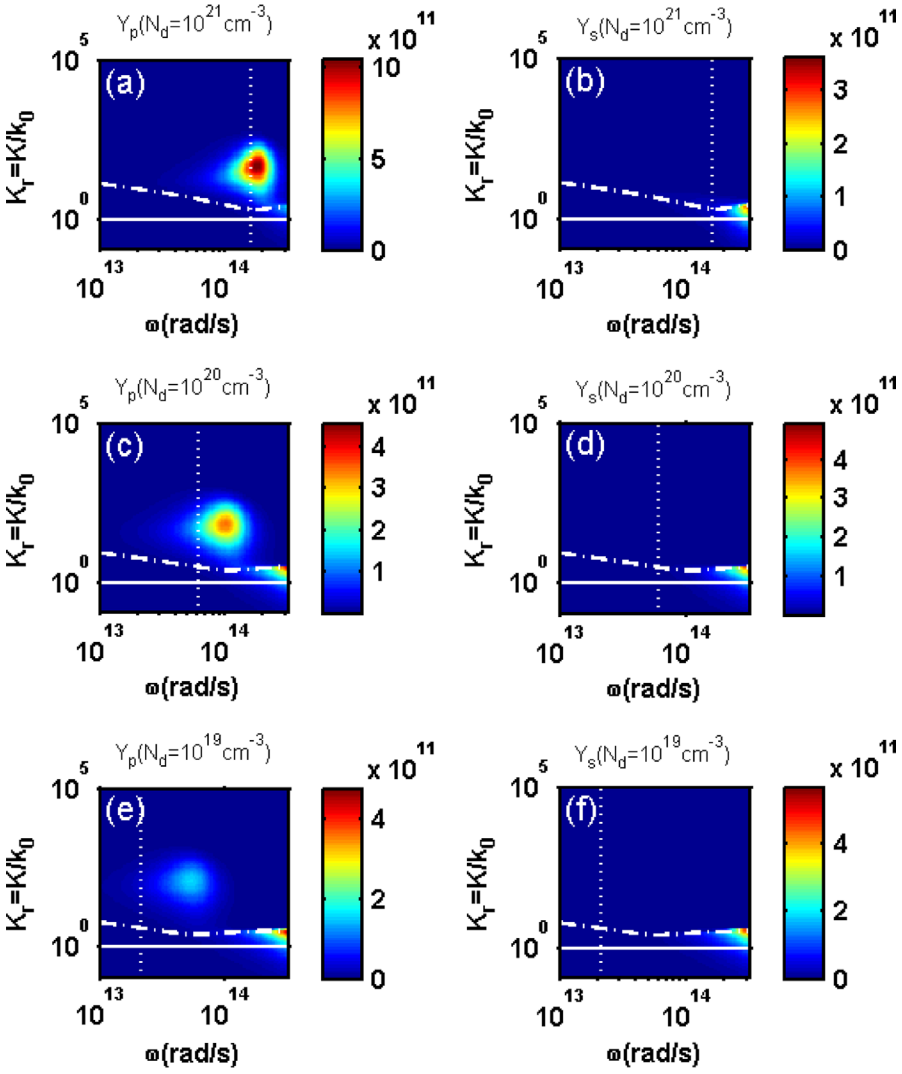

Fig. 5. The weighted TF of the radiative heat transfer between two doped bulk Si plates at different dopant concentrations. Y_p and Y_s correspond to the weighted TF for p and s polarizations, respectively.

which can greatly enhance radiative heat transfer [17]. Notice that the enhancement of near-field thermal radiation due to hyperbolic metamaterial has different mechanisms from that of a bulk material. It is the frustrated photon modes with large K that dominate in the hyperbolic metamaterial case, whereas the dominant photon modes in a bulk material are usually the evanescent photon modes.

We apply the Maxwell–Garnett (MG) theory to estimate the optical properties of our doped Si based metamaterials. Previously, the MG theory successfully predicted the infrared optical response of SiC nanowire arrays [9] and SiC nanohole arrays [20] for low filling ratios. When SiWAs or SiHAs perform as near-field thermal emitters/absorbers, we assume that the wires or holes all align in the z direction. SiWAs and SiHAs can be viewed as semi-infinite anisotropic metamaterials with $\epsilon_{par}, \epsilon_{vet}$ specified by the MG theory as

$$\epsilon_{par} = \epsilon_h \frac{\epsilon_i(1+f)+\epsilon_h(1-f)}{\epsilon_i(1-f)+\epsilon_h(1+f)}$$
$$\epsilon_{vet} = \epsilon_h(1-f)+\epsilon_i f, \tag{18}$$

where ϵ_h is the permittivity of the host material, and ϵ_i is the permittivity of the embedded material. f is the filling ratio that defines the percentage of the embedded material occupied in the host material. For SiWAs the host material is air while the embedded material is Si, and vice versa for SiHAs. Thus, for SiWAs, $\epsilon_h = \epsilon_0$ which is the permittivity of air and $\epsilon_h = \epsilon_{Si}$. For SiHAs, $\epsilon_h = \epsilon_{Si}, \epsilon_i = \epsilon_0$.

For the dopant concentration $N_d = 10^{20}\text{cm}^{-3}$, Re[$\epsilon_{par}$] and Re[$\epsilon_{vet}$] of SiWA and SiHA are plotted in Fig. 6(a) and (b) as a function of (ω, f). Here, we only plot the filling ratio f in the range of [0, 0.4] because the MG theory is valid only for low filling ratio cases. The effective material property diagrams of these two anisotropic metamterials are plotted in Fig. 6(c) and (d). Thus, we expect that SiWAs behave as a hyperbolic metamaterial when the photon frequency is below the plasma frequency, whereas SiHAs behave just like an anisotropic metal.

Based on the weighted LDOS formalism, we investigate the "near-field emissivity" of SiWA and SiHA structures. The weighted LDOS at the distance $d = 10$ nm above the SiWAs and SiHAs with the different filling ratios are plotted in Fig. 7. Compared with Fig. 3, we can see that the dominant photon modes of the near-field thermal radiation of SiWAs spread over a slightly wider frequency range than that of bulk Si, whereas there is almost no difference between the SiHA case and the bulk Si case. SiWAs are expected to behave as hyperbolic metamaterials, whose LDOS could be enhanced due to its broadband frustrated photon modes. However, in Fig. 7, when we plot the vertical white dotted line to separate the hyperbolic metamaterial characteristic (or metallic

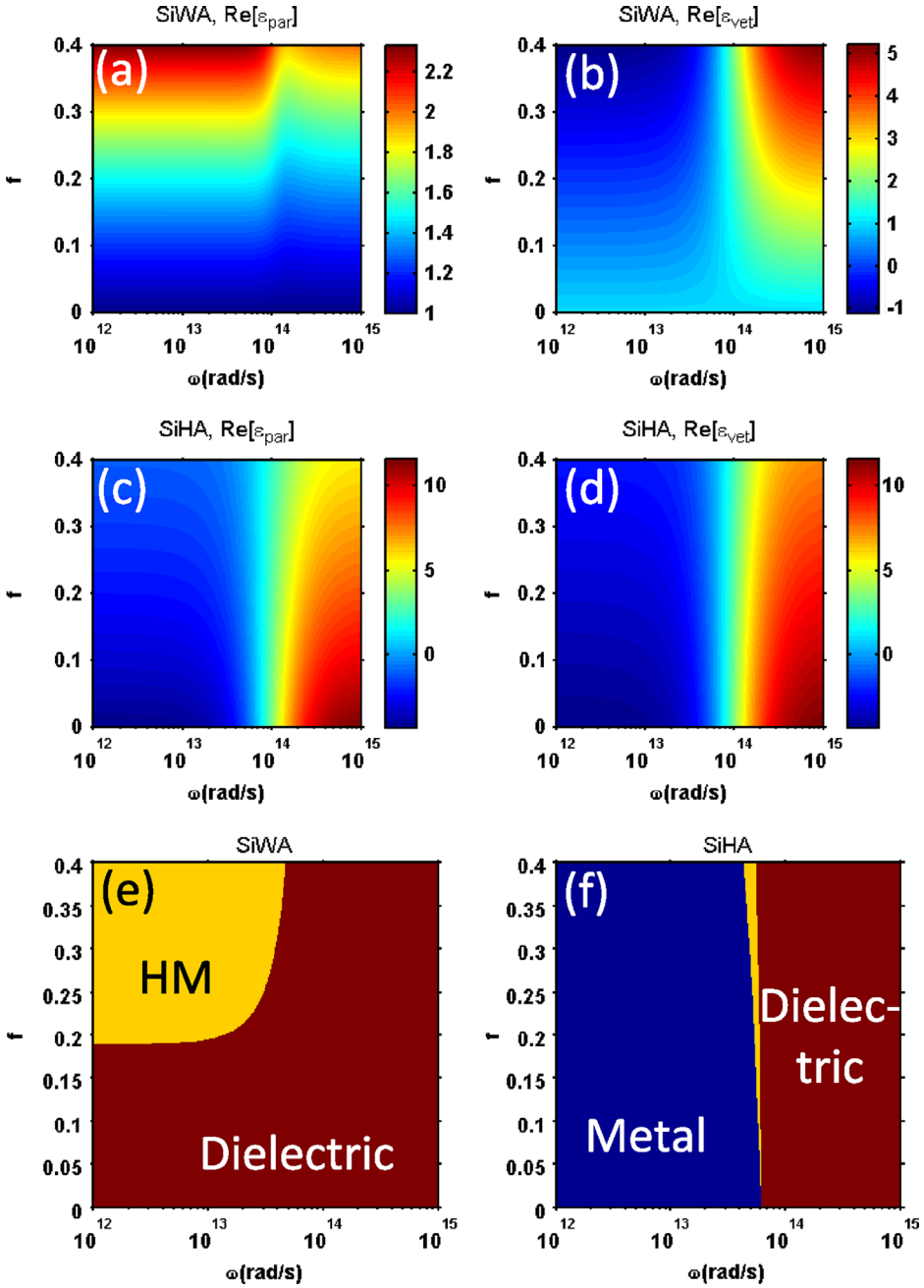

Fig. 6. (a) Real part of the parallel component and (b) real part of the vertical component of the effective permittivity of Si wire arrays (SiWA) in (ω, f) based on the Maxwell–Garnett theory. (c) and (d) the effective permittivity of Si hole arrays (SiHA) in (ω, f). (e) and (f) effective material property diagrams for SiWA and SiHA in (ω, f). "HM", "Dielectric" and "Metal" denote the regions of hyperbolic metamaterial characteristic with $(\epsilon_{par} > 0, \epsilon_{vet} < 0)$, dielectric characteristic with $(\epsilon_{par} > 0, \epsilon_{vet} > 0)$, and metallic characteristic with $(\epsilon_{par} < 0, \epsilon_{vet} < 0)$, respectively. The dopant concentration of Si is $N_d = 10^{20}\,\mathrm{cm}^{-3}$.

characteristic for SiHAs) and dielectric characteristic of SiWAs, we find that the dominant photon modes of SiWA lie in the dielectric characteristic region, which corresponds to $(\epsilon_{par} > 0, \epsilon_{vet} > 0)$. Thus, the near-field thermal radiation of SiWAs is not dominated by its hyperbolic metamaterial characteristic. The reason why the hyperbolic metamaterial characteristic fails to dominate the thermal radiation of SiWAs is also due to the very large imaginary part of the permittivity of doped Si. According to the dispersion relation of an anisotropic metamaterial described by Eq. (17), the incident photons with large K cannot be coupled into the propagating wave modes because k_z could have a very large imaginary part and therefore the wave modes are exponentially decaying. Similarly, for the SiHA cases, we also find that it is not the surface plasmon polariton wave modes that dominate the near-field heat transfer. Therefore, we can conclude that the dominant mechanism of the near field thermal radiation of SiWAs and SiHAs is the direct absorption of the incident evanescent photons from the induced dipoles in Si, which is similar to the case of bulk Si. However, due to the wire-array and hole-array nanostructures, the LDOS above the surface of SiWAs/SiHAs is different from the LDOS above the bulk doped Si.

Finally, the heat transfer coefficient for SiWA–SiWA cases and SiHA–SiHA cases at temperature $T = 300$ K and dopant concentration $N_d = 10^{20}\,\mathrm{cm}^{-3}$ are plotted in Fig. 8 as the function of vacuum gap size. Here, the heat transfer coefficient is defined as

$$h(T) = \frac{\partial \int_0^\infty \Phi(\omega, T) d\omega}{\partial T}. \tag{19}$$

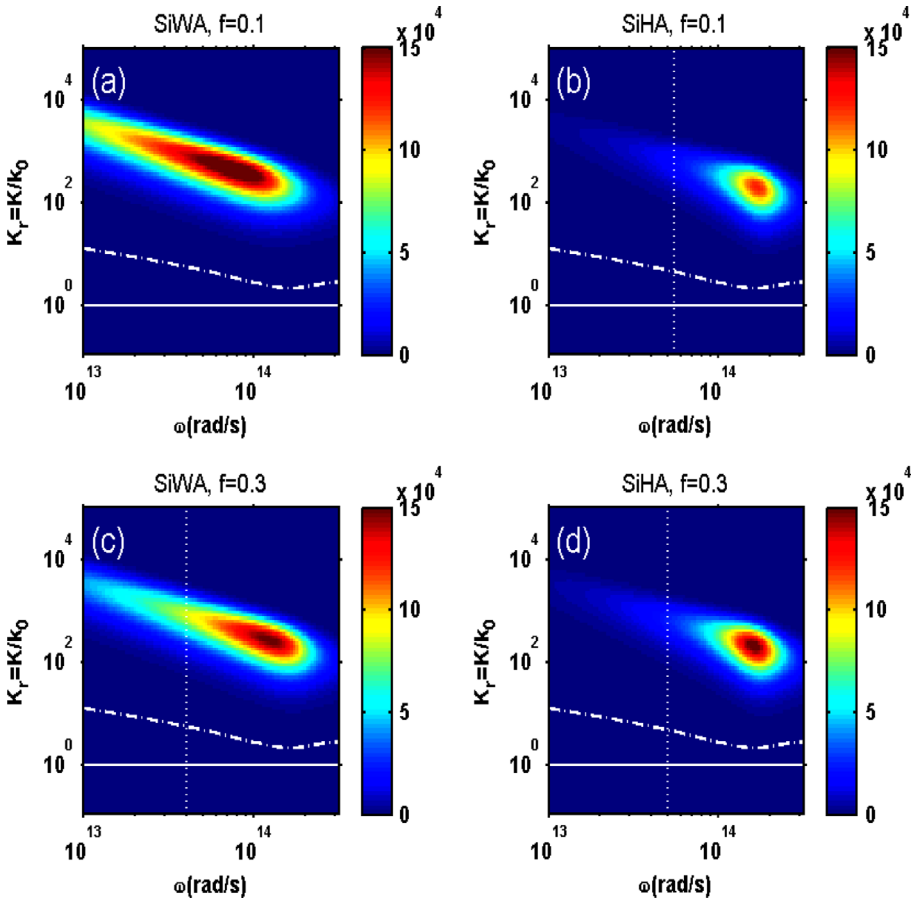

Fig. 7. The weighted LDOS of SiWA and SiHA with different dopant concentrations. Red vertical line denotes the boundary between the dielectric material property and the HM/metallic material property. (For interpretation of the references to color in this figure legend, the reader is referred to the web version of this article.)

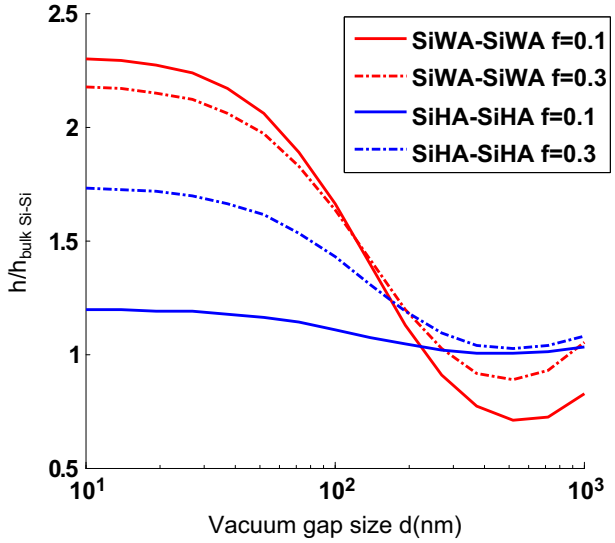

Fig. 8. The heat transfer coefficient at temperature $T=300$ K of the SiWA–SiWA cases and the SiHA–SiHA cases, normalized to the heat transfer coefficient of bulk Si–Si cases. The dopant concentration of Si is $N_d = 10^{20}\text{cm}^{-3}$.

We can see that the near field heat transfer of SiWA–SiWA and SiHA–SiHA cases have a factor of 2 enhancement in comparison with the bulk Si–Si case when the gap size is smaller than 100 nm. The heat transfer between SiWA and SiWA increases as the filling ratio decreases, whereas the heat transfer between SiHA and SiHA increases with increasing filling ratio. Notice that, in comparison with the metal nanowire array case mentioned in [17], even though the doped Si appears like a metal (the real part of its permittivity is negative at the frequencies below the plasma frequency), the near field heat radiation of SiWAs fails to have orders of magnitude enhancement than that of the bulk material. This is because the large imaginary component of the permittivity of doped Si mitigates the hyperbolic metamaterial characteristics of SiWAs.

6. Conclusion

In this paper, we studied the near-field radiative properties of two types of Si based metamaterials (SiWAs and SiHAs) by changing dopant concentrations of Si and the filling ratio of nanowires or nanoholes. In particular, SiWAs were used to design hyperbolic metamaterials but did not show significant enhancement for near-field radiative heat transfer because of the large imaginary component of the permittivity of doped Si. The dominant heat transfer mechanism for SiWA–SiWA and SiHA–SiHA is the direct absorption of the incident evanescent photons from the induced dipoles in Si, which is similar to the case for Si–Si. The near-field radiative heat transfer between SiWAs and SiHAs is larger than the one between two Si plates at small gaps. Tunable Si based metamaterials can be used as novel near-field photonic materials which have potential applications in thermophotovoltaic energy conversion, thermal management, and photothermal technologies.

Acknowledgments

This work is supported by the National Science Foundation (CBET-1253692).

References

[1] D.R. Smith, J.B. Pendry, M.C.K. Wiltshire, Science (New York, N.Y.) 305 (2004) 788.
[2] C.M. Soukoulis, M. Wegener, Nat. Photon. 5 (2011) 523.
[3] Y. Liu, X. Zhang, Chem. Soc. Rev. 40 (2011) 2494.
[4] S.M. Rytov, Y.A. Kravtsov, V.I. Tatarskii, Principles of Statistical Radiophysics, vol. 3, Springer-Verlag, 1989, (in English). ISBN-10: 0387178295, ISBN-13: 978-0387178295 ⟨http://www.amazon.com/Principles-Statistical-Radiophysics-S-Rytov/dp/0387178295⟩.
[5] S. Basu, Z.M. Zhang, C.J. Fu, Int. J. Energy Res. 33 (2009) 1203.
[6] K. Joulain, J.-P. Mulet, F. Marquier, R. Carminati, J.-J. Greffet, Surf. Sci. Rep. 57 (2005) 59.
[7] S.-A. Biehs, E. Rousseau, J.-J. Greffet, Phys. Rev. Lett. 105 (2010) 234301.
[8] S. Shen, A. Narayanaswamy, G. Chen, Nano Lett. 9 (2009) 2909.
[9] S.-A. Biehs, M. Tschikin, P. Ben-Abdallah, Phys. Rev. Lett. 109 (2012) 104301.
[10] S. Basu, Z.M. Zhang, J. Appl. Phys. 105 (2009) 093535.
[11] J.B. Pendry, J. Phys.: Condens. Matter 11 (1999) 6621.
[12] C.J. Fu, Z.M. Zhang, Int. J. Heat Mass Transfer 49 (2006) 1703.
[13] T.K. Gaylord, J.N. Linxwiler, Am. J. Phys. 44 (1976) 353.
[14] W.E. Beadle, J.C.C. Tsai, R.D. Plummer, Quick Reference Manual for Silicon Integrated Circuit Technology, Jonh Wiley & Sons, New York, NY, 1985.
[15] R.S. Ottens, V. Quetschke, S. Wise, a.a. Alemi, R. Lundock, G. Mueller, D. H. Reitze, D.B. Tanner, B.F. Whiting, Phys. Rev. Lett. 107 (2011) 014301.
[16] C. Chen, P. Berini, D. Feng, S. Tanev, V. Tzolov, Opt. Express 7 (2000) 260.
[17] B. Liu, S. Shen, Phys. Rev. B 87 (2013) 115403.
[18] Y. Guo, C.L. Cortes, S. Molesky, Z. Jacob, Appl. Phys. Lett. 101 (2012) 131106.
[19] J. Pendry, Opt. Photon. News 15 (2004) 32.
[20] S.-A. Biehs, P. Ben-Abdallah, F.S.S. Rosa, K. Joulain, J.-J. Greffet, Opt. Express 19 (2011) A1088.